DOI: 10.1002/cmdc.200500009

Selective Indole-Based ECE Inhibitors: Synthesis and Pharmacological Evaluation

Michael Brands,[a] Jens-Kerim Ergüden,[a] Kentaro Hashimoto,*[a] Dirk Heimbach,[a] Thomas Krahn,[a] Christian Schröder,[b] Stephan Siegel,[a] Johannes-Peter Stasch,[a] Hideki Tsujishita,[c] Stefan Weigand,[d] and Nagahiro H. Yoshida[e]

Inhibition of the metalloprotease ECE-1 may be beneficial for the treatment of coronary heart disease, cancer, renal failure, and urological disorders. A novel class of indole-based ECE inhibitors was identified by high throughput screening. Optimization of the original screening lead structure ***6*** *led to highly potent inhibitors such as* ***11****, which bears a bisaryl amide moiety linked to the indole C2 position through an amide group. Docking of* ***11*** *into a model structure of ECE revealed a unique binding mode in which the Zn center of the enzyme is not directly addressed by the inhibitor, but key interactions are suggested for the central amide group. Testing of the lead compound* ***6*** *in hypertensive Dahl S rats resulted in a decrease in blood pressure after an initial period in which the blood pressure remained unchanged, most probably the result of ET-1 already present. Indole derivative* ***6*** *also displays a cardio-protective effect in a mouse model of acute myocardial infarction after oral administration. The more potent chloropyridine derivative* ***9*** *antagonizes big-ET-1-induced increase in blood pressure in rats at intravenous administration of 3 mg kg^{-1}. All ECE inhibitors of the indole class showed high selectivity for ECE over related metalloproteases such as NEP and ACE. Therefore, these compounds might have further potential as drugs for the treatment of coronary heart diseases.*

Introduction

The discovery of endothelin (ET-1) and its potent vasoconstrictive activity[1,2] marks the beginning of a remarkable race toward an understanding of the therapeutic implications of the endothelin system and the benefit of its blockade for the treatment of several diseases. Counterintuitively, ET-1 levels are not elevated in patients of primary hypertension[3] (except in African Americans[4]) and in patients with stable coronary diseases. However, elevated plasma ET-1 levels are associated with numerous complications that frequently occur in patients with coronary heart diseases (CHD) such as arrhythmia[5] and myocardial infarction.[6] Elevated ET-1 levels have been linked to the presence of chronic inflammation as it is currently understood for the early phases of atherosclerotic plaque formation.[7] Patients suffering from pulmonary hypertension display elevated ET-1 levels in their lungs.[8] Increased plasma ET-1 concentrations in patients suffering form congestive heart failure (CHF) have led to numerous clinical investigations of drugs that block the activity of ET-1.[9,10] In addition, endothelin has also been linked to diseases outside those related to CHD and CHF; the mitogenic activity of ET-1 has led to numerous studies of endothelin-blocking agents in several cancer indications, primarily prostate cancer.[11,12] Renal failure has also been linked to overexpression of the endothelin system.[13] Recently, results from an animal study revealed that inhibition of endothelin formation is beneficial in the treatment of urological disorders such as benign prostatic hyperplasia.[14]

The endothelin system itself exerts a high level of complexity for both the induction of formation of ET-1 and for the pathways through which ET-1 acts. ET-1 interacts primarily with its corresponding receptors ET_A and ET_B. It remains controversial whether antagonists of the ET_B receptor are detrimental or beneficial, as one of the receptor functions is the pulmonary clearance of ET-1.[9] The vasoconstrictive effect of ET-1 is mediated primarily through the ET_A receptor, which consequently became the focus of efforts to develop endothelin receptor antagonists. Those endeavors led to the approval of bosentan for the treatment of pulmonary hypertension in 2001.[15–17] Anoth-

[a] *Dr. M. Brands, Dr. J.-K. Ergüden, K. Hashimoto, Dr. D. Heimbach, Dr. T. Krahn, Dr. S. Siegel, Dr. J.-P. Stasch*
Bayer HealthCare AG, Business Group Pharma
Research & Development
Aprather Weg 18a, 42096 Wuppertal (Germany)
Fax: (+49) 202-36-4061
E-mail: kentaro.hashimoto@bayerhealthcare.com

[b] *Prof. Dr. C. Schröder*
FH Lausitz University of Applied Sciences
Department of Biological, Chemical and Process Engineering
P.O.B. 1538, 09158 Senftenberg (Germany)

[c] *Dr. H. Tsujishita*
Current address:
Shionogi & Co., Ltd., 5-12-4 Sagisu Fukushima-ku, Osaka, 553-0002 (Japan)

[d] *Dr. S. Weigand*
Current address:
Roche Diagnostics GmbH, Pharma Research, 82377 Penzberg (Germany)

[e] *Dr. N. H. Yoshida*
Current address:
Bayer Yakuhin, Ltd., 3-5-36 Miyahara Yodogawa-ku, Osaka, 532-8577 (Japan)

er advanced agent, the more ET_A-selective receptor antagonist atrasentan, is currently in pre-registration for the treatment of hormone-refractory prostate cancer.[12]

As the downstream effects of endothelin are complex in nature and, in some cases (such as CHF), therapeutic intervention has produced disappointing clinical results, newer approaches target the formation of ET-1. The 21-residue polypeptide is formed by proteolytic cleavage from its inactive precursor big-ET-1. This cleavage is mediated by endothelin converting enzyme (ECE),[18] which is a metalloprotease bearing a Zn catalytic center. This enzyme is structurally related to neutral endopeptidase (NEP), an enzyme that catalyzes the degradation of ANP (atrial natriuretic peptide). As the inhibition of NEP has been associated with the accumulation of ET-1, the latest efforts are focused on the identification of selective ECE inhibitors that do not block NEP.[19,20] Figure 1 shows some published selective and potent ECE inhibitors. CGS 35066[21] is the result of an optimization program starting with a peptidic structure. It exhibits a typical protease-binding structural motif: a phosphonate group. A similarly strong thiol group pharmacophore is present in RO 67-7447,[22] whereas the inhibitor SM-19712[23] of Sumitomo appears to bind the catalytic center of the enzyme with the sulfonyl urea group. Pharmacological activity was reported in a standard model (decrease in blood pressure after intravenous injection of big-ET-1 in rats) for CGS 35066[21] and SM-19712.[23] However, the typical structural elements required for binding to the catalytic center can render metabolic stability and absorption after oral administration problematic. Thus, activity by the oral route of administration has been reported only for prodrugs of CGS 35066[24] and RO 67-7447.[22] Therefore, there is still a need for the discovery of novel and selective lead structures for the inhibition of ECE.

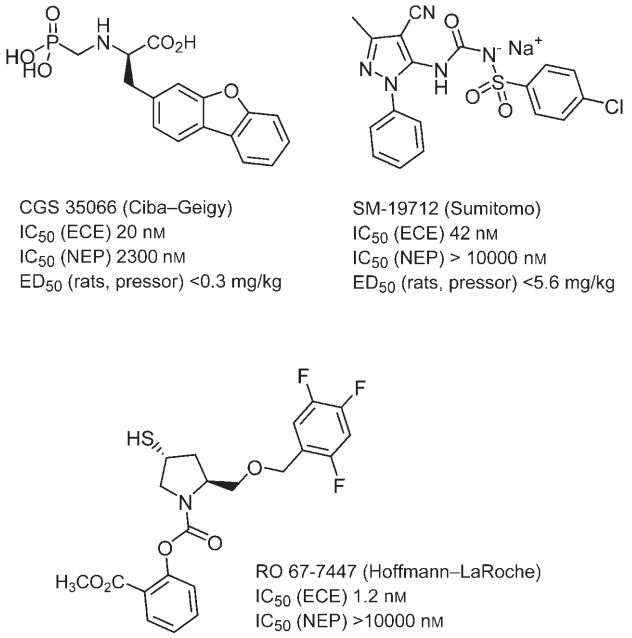

Figure 1. Selected published ECE inhibitors.

By screening of the Bayer compound collection, indole derivative **6** was identified as a potent ECE inhibitor (Scheme 1).[25] Under a standard enzyme-linked immunosorbent assay (ELISA) format, **6** revealed an IC_{50} value of 1.8 μM. The compound showed no inhibitory effect against the related metalloproteases NEP and ACE at concentrations up to 100 μM. The interesting in vitro activity, unprecedented structure, and high selectivity observed for this compound rendered indole **6** an attractive lead structure that is well-suited as a starting point for a medicinal chemistry optimization program. Herein, we disclose details of the synthesis, SAR, and proposed binding mode of **6** and optimized analogues thereof, along with pharmacokinetic and pharmacology data.

Chemistry

The lead structure **6** was prepared according to the procedure outlined in Scheme 1. Commercially available ethyl 5-nitro-1*H*-indole-2-carboxylate **1** was treated with 2-fluorobenzylbromide, followed by standard reduction of the nitro group and treatment with pivaloyl chloride to give amide **4** as a central building block. Saponification of the ester and amide formation with aniline yielded the lead structure **6**. The use of differ-

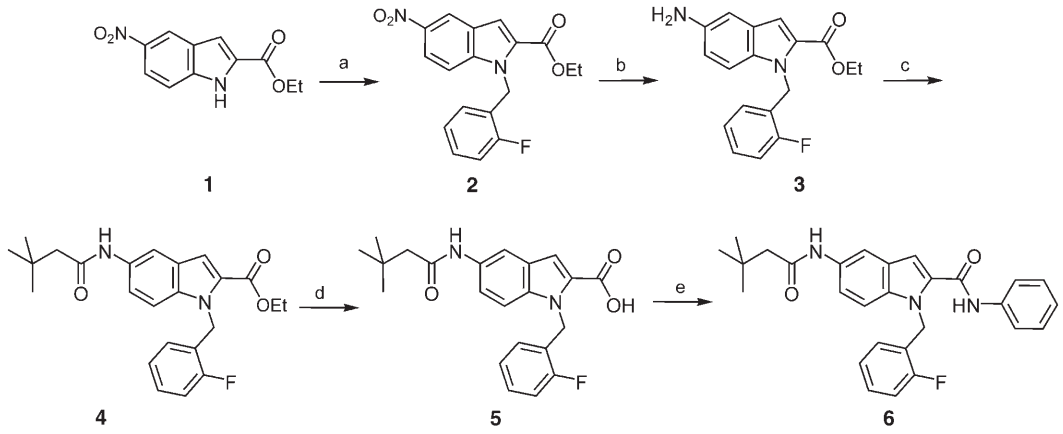

Scheme 1. a) KO*t*Bu, 18-crown-6, 0 °C, 2-fluorobenzylbromide, THF, RT, 75 %; b) Pd/C, $(NH_4)(HCO_2)$, EtOH/EtOAc, 95 %; c) $(CH_3)_3CCH_2COCl$, NEt_3, CH_2Cl_2, 0 °C→RT, 53 %; d) LiOH, MeOH/H_2O (3:1), RT, 96 %; e) EDCI, DMAP, DMF, aniline, RT, 60 %. DMAP = 4-dimethylaminopyridine, DMF = *N*,*N*-dimethylformamide, EDCI = 1-(3-dimethylaminopropyl)-3-ethylcarbodiimide hydrochloride.

ent aromatic and heteroaromatic amines allowed the introduction of variations in the C2 amide side chain to yield derivatives **7**–**11** (Table 1).

Table 1. Inhibition of ECE-mediated cleavage of big-ET-1 by compounds **6**–**14**.

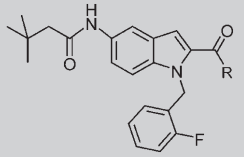

Compound	R	IC_{50} [nM]
6		1800
7	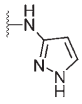	> 10000
8	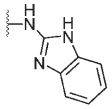	> 10000
9	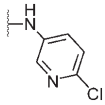	220
10	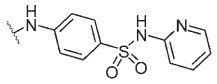	410
11	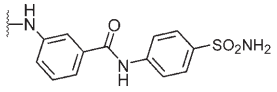	10
13	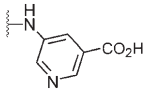	180
14	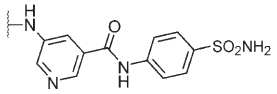	10

In the course of the SAR work, it was found that a bisaryl amide side chain attached to the C2 position of the indole skeleton and that replacement of the phenyl ring of the C2 amide by pyridine led to ECE inhibitors with improved activity (see below). The combination of these structural features is outlined in the synthesis of derivative **14** in Scheme 2. 5-Aminonicotinic acid methyl ester was treated with key intermediate **5** to yield amide **12**. Saponification of the methyl ester provided derivative **13**, and amide coupling with HATU as a coupling agent afforded bisaryl amide **14**.

Structure–Activity Relationship Studies

Clearly the next step for the medicinal chemistry program was to identify pharmacophore patterns in the structure of screening lead **6** that are suited to interact with the catalytic center of ECE. As compound **6** lacks any structural elements that can bind or chelate the Zn center of ECE, a systematic approach was needed to elucidate putative binding motifs. An added goal of the optimization program was to improve the in vitro activity of **6** (IC_{50} = 1.8 μM) by lowering the IC_{50} value into the nanomolar range. However, as described earlier,[26] variations in the side chains attached to the indole skeleton at the N1 and C5 positions did not give rise to compounds with improved activity. For this reason, it was hypothesized that these moieties bind a corresponding pocket of the enzyme with high affinity. Although some initial attempts to replace the phenyl group attached to the C2 position of the indole through an amide linker by various heterocycles yielded inactive derivatives **7** and **8** (Table 1), the introduction of a 3-pyridyl residue resulted in an improved activity toward ECE. Moreover, the presence of further substituents like chlorine (in **9**) or a carboxylate group (in **13**) was tolerated. Compound **13** served as the starting point for a second-generation approach through which a 20-fold improvement in activity in vitro was identified by the introduction of a second aryl amide bearing a primary sulfonamide group in the *para* position (**14**, IC_{50} = 10 nM). This finding could be transferred to the series bearing a phenyl group

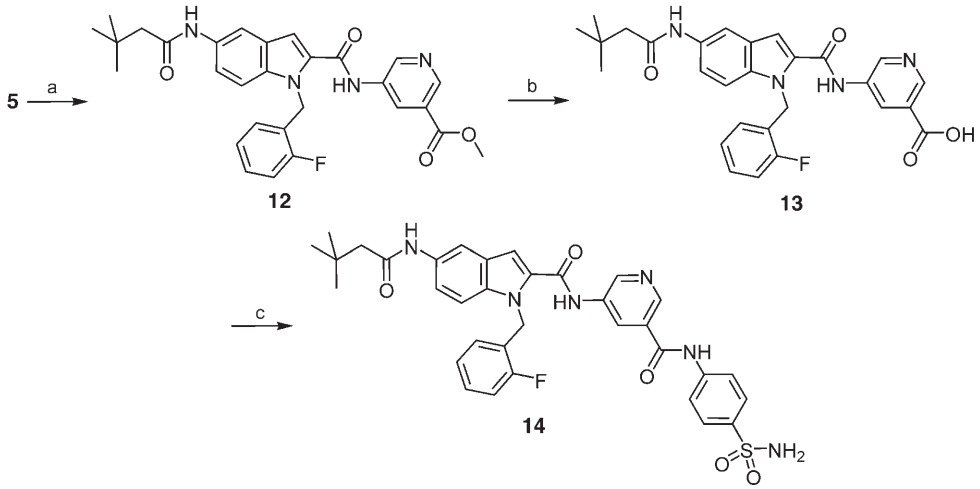

Scheme 2. a) 5-aminonicotinic acid methyl ester, DMAP, HATU, DMF, RT, 61%; b) LiOH, MeOH/THF/H_2O, 90 °C, 90%; c) sulfanylamide, HATU, DMAP, DMF, RT, 53%. DMAP = 4-dimethylaminopyridine. HATU = *O*-(7-azabenzotriazol-1-yl)-*N*,*N*,*N*′,*N*′-tetramethyluronium hexafluorophosphate.

at C2 of the indole amide group without loss of in vitro activity, as with compound **11**. Finally, the amide linker between the two aryl groups was preferred over a sulfonamide group, as exemplified by compound **10**.

Key representative compounds such as **6**, **9** and **11** were assessed for their inhibitory potential toward other metalloproteases. Inhibition of NEP and ACE was not observed for these compounds at concentrations of up to 100 μM. Thus, the indole class provides ECE inhibitors with exceptionally high selectivity.

To gain insight into the underlying reason for the favorable selectivity profile and binding mode of the indole-based ECE inhibitors, a computational chemistry model of the binding mode of compound **11** was established. Unfortunately, a high resolution X-ray crystallographic structure of the human ECE homolog (hECE-1) is not available. Therefore, a homology model of ECE was created by using the X-ray crystallographic structure of the NEP–phosphoramidon complex (PDB: 1DMT) as a template, similar to an approach reported by Bur et al.[27] This model was used to dock the structures of the known weak ECE inhibitor phosphoramidon (IC_{50} = 3.5 μM) and the potent indole-based inhibitor **11** (IC_{50} = 10 nM). In agreement with published results,[27] phosphoramidon binds to the Zn center of the enzyme through the phosphonamide function (Figure 2). Another strong interaction is made through hydrogen bonding between Arg 738 and the leucine carbonyl oxygen atom of phosphoramidon. Finally, the tryptophan indole moiety binds the C^{α} backbone carbonyl group of ECE Val 565 through its N–H group and undergoes a π-stacking interaction with Phe 149. There is a considerable difference between the NEP and ECE amino acid sequences that form the S2′ pocket. The S2′ pocket in ECE seems more open, and it has been speculated[27] that the lower affinity phosphoramidon has toward ECE than for NEP results from a weaker interaction between its indole group and the S2′ pocket of ECE.

Interestingly, docking of the ECE inhibitor **11** into the model structure of ECE resulted in placement of the indole moiety in a location similar to that observed for the tryptophan residue of phosphoramidon to create a similar π-stacking interaction with Phe 149 (Figure 3). Clearly, no interaction to Val 565 is possible, as the indole nitrogen atom bears a substituent. However, the 2-fluoro benzyl substituent is observed to fit tightly into the S3′ pocket, which explains why SAR does not tolerate variations at this position.[26] No major interaction is observed for the amide group directly attached to the 2 position of the indole. However, the amide motif that connects the two phenyl rings in the C2 side chain is thought to interact with His 732 and Ala 567 through hydrogen bonds and is therefore regarded as a central pharmacophore. As the model does not predict any direct interaction between the indole-based inhibitor and the Zn center, the binding of the bisaryl amide motif seems to be responsible for the higher binding affinity observed for inhibitor **11** relative to the screening lead **6**. Finally, an additional interaction is predicted between the sulfonamide group and Gln 616. The model also explains the inactivity of **7** and **8**. Whereas the polar pyrazole moiety of **7** is unable to directly contact the catalytic Zn^{2+} ion, the benzimidazole of **8** is simply too bulky to fit into the S1′ pocket.

Overall, the model is able to provide a rationale for the observed SAR trends for the indole-type inhibitors.[26] It highlights the pharmacophore character of the central amide group of the bisaryl amide side chain binding to His 732 and Ala 567 of the ECE backbone without interacting directly with the Zn center. Although located close to a solvent-exposed area, the sulfonamide group of **11** makes additional interaction with the enzyme which renders **11** a highly effective ECE inhibitor.

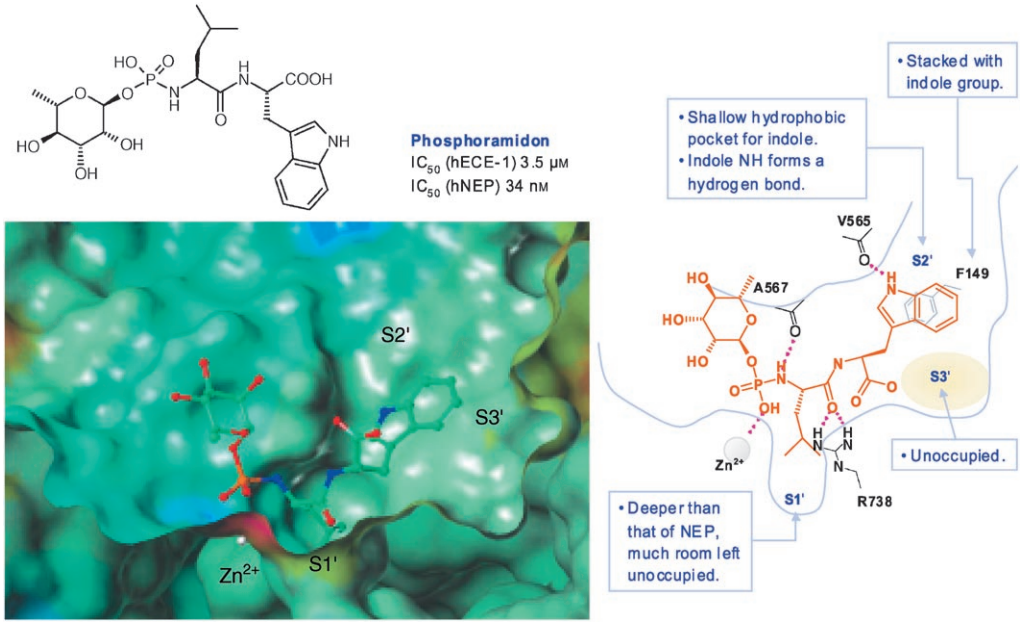

Figure 2. Model for the binding of phosphoramidon to the catalytic site of human ECE-1 (hECE-1) constructed from the X-ray crystallographic structure data from human NEP (hNEP) 24.11.

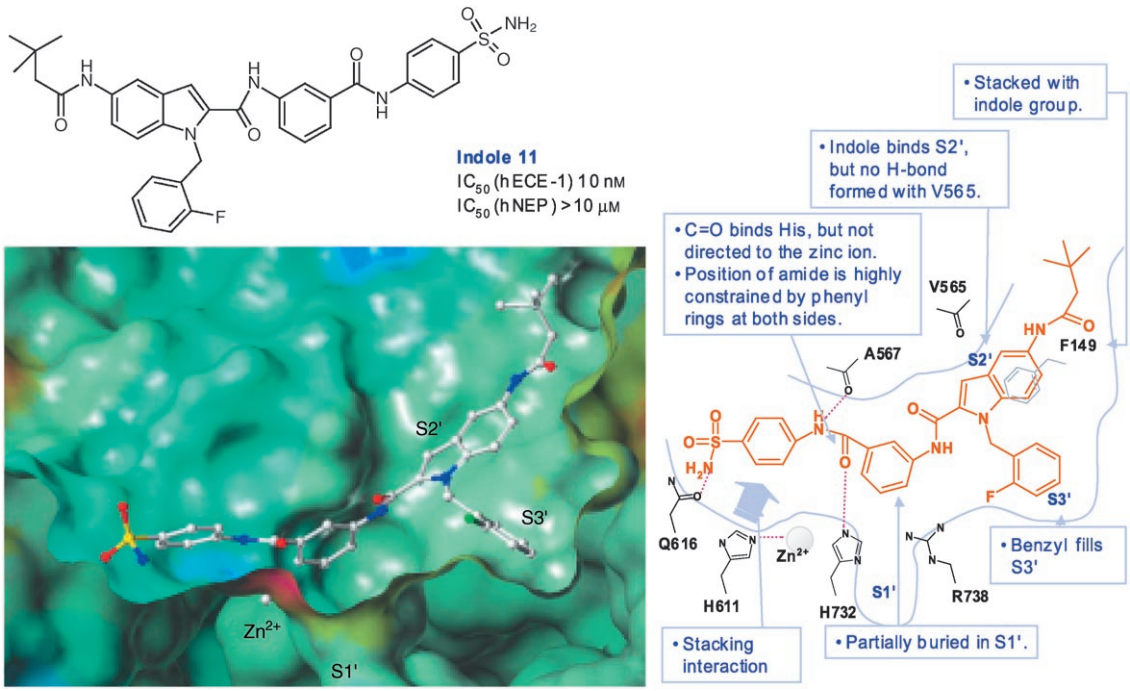

Figure 3. Predicted binding mode of indole-based inhibitor **11** to the catalytic site of hECE-1 constructed from the X-ray crystallographic structure data from human NEP (hNEP) 24.11.

Pharmacology/Pharmacokinetics

The pharmacokinetic properties of compounds from the indole class of ECE inhibitors were studied in rats to assess their suitability for in vivo pharmacology model studies. Rats were treated with inhibitors **6** and **9** at 1 mg kg^{-1} intravenously and 10 mg kg^{-1} orally (solution in Solutol HS 15/ethanol/water 40:10:50) and plasma samples were collected over 24 h. As summarized in Table 2, the pharmacokinetic parameters are quite different between the compounds. Inhibitor **6** shows a low clearance and low volume of distribution after intravenous administration. The compound is systemically available after oral administration with a bioavailability of 21%. In contrast, compound **9** proved to be a high-clearance drug with a high volume of distribution and low oral availability. Furthermore, compound **11**, a representative from the bisaryl amide subclass, was studied and was found to exhibit no oral availability at all. The lack of exposure after oral administration can be explained by the relatively high molecular weight and high polar surface area (144 Å^2 for **11** compared with 65 Å^2 for compound **9**), which are widely accepted descriptors for the likelihood of absorption.[28] As indoles **6** and **9** exhibited systemic exposure after both intravenous and oral administration over a considerable time period, they were both studied in various pharmacology models to establish a proof-of-principle for this novel compound class.

The acute blood-pressure-lowering effects of ECE inhibitor **6** were investigated in salt-loaded Dahl S (salt-sensitive) and Dahl R (salt-resistant) rats. The Dahl S rats develop hypertension, whereas the Dahl R rats stay normotensive under the 5-week high-salt diet (8% NaCl).[29] In certain tissues, the expression of prepro-ET-1 mRNA and ET-1 is increased in Dahl S but not in Dahl R rats.[30] As shown in Figure 4, ECE inhibitor **6** demonstrated a significant decrease in blood pressure in Dahl S rats at 3 mg kg^{-1} intravenous, whereas no blood-pressure-lowering effect was observed in the Dahl R rats. Notably, the blood-pressure-lowering effect of **6** was observed only after an induction period of approximately 30 min after treatment. In contrast, the selective ET_A receptor antagonist (FR 139317)[31] used in the same model effected a decrease in blood pressure directly after administration. It may be hypothesized that this difference in time course results from the need for ET-1 already present in the blood to be consumed or degraded before the effect of an ECE inhibitor becomes apparent. On the other hand, blockade of the endothelin receptor becomes effective immediately after administration and leads to a faster effect in this particular model. As compound **6** was shown to yield measurable plasma levels over 4 h when administered at doses of 20 or

Table 2. Pharmacokinetic properties of compounds **6** and **9**.

Compound	Intravenous (1 mg kg^{-1})			Oral (10 mg kg^{-1})		
	$t_{1/2}$ [h]	V_{ss} [L]	$C_{L,\ blood}$ [L kg^{-1} h^{-1}]	$C_{max,\ norm}$ [mg L^{-1}] at time-point (h)	AUC_{norm} [kg h L^{-1}]	Bioavailability [%]
6	1.04	0.81	1.22	27 (4)	0.244	21
9	2.16	8.38	4.44	1.5 (1)	0.01	5

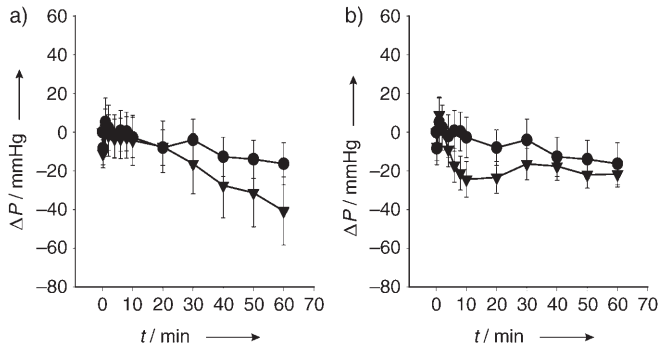

Figure 4. Deviations in mean blood pressure (ΔP) in Dahl S rats effected by a) ECE-1 inhibitor **6** (●: vehicle, $n=5$; ▼: 3 mg kg^{-1} intravenous, $n=6$) and b) ET_A antagonist FR 139317 (●: vehicle, $n=5$; ▼: 10 mg kg^{-1} intravenous, $n=7$).

50 mg kg^{-1} orally, effects on survival were assessed in a mouse acute MI model (Experimental Section). At a dose of 50 mg kg^{-1}, **6** yielded a survival rate of 80% (compared with 20% in the untreated control group). Thus, **6** proved active in vivo in two different models through intravenous and oral application.

Unfortunately, compound **6** failed to demonstrate efficacy in a standard model used for the in vivo evaluation of ECE inhibitors. In this model, rats were treated with the ET-1 precursor big-ET-1 by intravenous injection, which leads to a fast and pronounced blood pressure increase due to the cleavage of big-ET-1 by ECE. This so-called pressor effect peaks within a timeframe of 10 to 30 min following the administration of big-ET-1. Inhibitor **9** was tested side by side with the described ECE inhibitor SM-19712. As depicted in Figure 5, compound **9** showed a significant effect at a dose of 3 mg kg^{-1}, whereas a higher dose of 10 mg kg^{-1} was needed for SM-19712 to result in a significant effect.

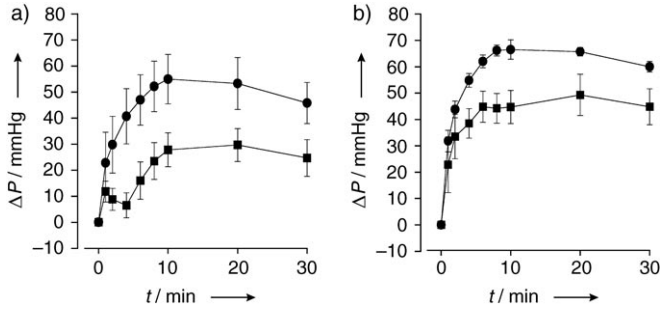

Figure 5. Big-ET-1-induced blood pressure model in rats: effects of a) SM-19712 (●: big-ET-1 (9 μg kg^{-1} intravenous), $n=4$; ■: big-ET-1 + SM-19712 (10 mg kg^{-1} intravenous), $n=4$) and b) inhibitor **9** (●: big-ET-1 (9 μg kg^{-1} intravenous), $n=4$; ■: big-ET-1 + indole **9** (3 mg kg^{-1} intravenous), $n=4$) toward mean blood pressure ΔP as a function of time after the administration of big-ET-1.

Conclusions

After some ET receptor antagonists have advanced as therapeutic principles to the market (bosentan for pulmonary hypertension) or into the approval process (atrasentan for hormone refractory prostate cancer), ECE inhibitors are currently being studied in preclinical models with the hope that they will be able to overcome some of the disadvantages observed with ET receptor antagonists in clinical studies for indications such as CHF. Several highly active and selective ECE inhibitors have been described (Figure 1), yet some bear functional groups like thiols or phosphonates which are typically required for tight binding to the Zn center in the ECE catalytic binding site. Such groups can be detrimental in regard to metabolic stability and oral absorption. None of these functional groups are found in the indole class of ECE inhibitors. Compounds derived from chemical optimization of the initial screening lead **6** ($IC_{50}=1800$ nM) show inhibitory effects on ECE in the nanomolar concentration range, as observed with chloropyridine **9** ($IC_{50}=220$ nM) and sulfonamide **11** ($IC_{50}=10$ nM). All compounds assessed so far, including **6**, **9**, and **11**, were highly selective for ECE and showed no inhibition of ACE and NEP at concentrations up to 100 μM.

Based on a homology model of ECE created with an X-ray crystallographic structure of NEP as a template, indole-based inhibitor **11** shows a unique binding mode that lacks a direct interaction with the Zn center of ECE. Instead, considerable binding affinity seems to result from interactions between the central amide motif of the bisaryl amide group and the sulfonamide attached to the terminal aryl group. Tight binding of the 2-fluoro benzyl group might explain the observed high selectivity against other metalloproteases.

Compounds **6** and **9** show systemic exposure in rats after oral administration and were therefore advanced to testing in pre-clinical models suited to assess their inhibitory activity toward ECE in vivo. Unfortunately, the highly active inhibitor **11** failed to generate any appreciable plasma ET-1 concentrations after oral administration, which is most likely the result of low absorption as a consequence of its high polar surface area.

Indole **6** decreases blood pressure in hypertonic Dahl S rats at a dose of 3 mg kg^{-1} given intravenously. The delayed onset of activity is in agreement with the mode of action, which requires the consumption of pre-existing ET-1 before the blockade of ECE and the inhibition of the de novo formation of the vasoconstrictor ET-1 can take effect. In contrast, a selective ET_A receptor antagonist elicits its effect immediately after intravenous administration. ECE inhibitor **6** has proven its cardio-protective effect after oral administration in a mouse model of acute myocardial infarction.

Indole **9** is effective in a standard rat pressor model that assesses the ability of ECE inhibitors to block the blood pressure increase mediated by intravenous injections of big-ET-1. Indole **9** has a minimal efficacious dose of 3 mg kg^{-1} and is therefore slightly more active than the inhibitor SM-19712, which was used as a positive control.

In summary, indoles **6** and **9** are novel ECE inhibitors that represent an unprecedented structural class; they display a unique binding mode to ECE. Their efficacy in target-related and disease models has been proven. Therefore, these compounds might have further potential as drugs for the treatment of coronary heart diseases.

Experimental Section

General methods: Melting points were determined with a Büchi B-545 melting point apparatus and were uncorrected. ^{1}H NMR spectra were recorded on a Bruker 500 UltraShield (500 MHz for ^{1}H) spectrometer in [D$_6$]DMSO with tetramethylsilane (TMS) as an internal standard. MALDI-TOF HR MS data were obtained with a Finnigan MAT 95. LC–MS data were collected by using a Micromass Platform LC with a Phenomenex Synergi 2μ Hydro-RP column ($\varnothing$ = 4.0 mm, l = 20 mm) and a gradient mixture of acetonitrile/water (9:1→0.5:9.5) at a flow rate of 1–2 mL min^{-1}. Purification was performed by preparative HPLC by using HP 1000 with a Kromasil 100 RP-18 column ($\varnothing$ = 2.1 mm, l = 60 mm) and a gradient mixture of acetonitrile/water (9:1→0.2:9.8) at a flow rate of 0.75 mL min^{-1}. All reagents and solvents purchased were the highest grade possible and were used without further purification.

2: Ethyl 5-nitro-1*H*-indole-2-carboxylate (**1**, 2.50 g, 10.7 mmol) and potassium *tert*-butoxide (1.44 g, 12.8 mmol) were added to a solution of 18-crown-6 (0.28 g, 1.07 mmol) in THF. The mixture was stirred at room temperature for 15 min followed by the addition of 2-fluorobenzylbromide (2.02 g, 10.7 mmol) in THF under cooling with an ice bath. After complete addition, the solution was allowed to stir at room temperature for 2 h. After the addition of water and phase separation, the aqueous layer was extracted with EtOAc three times. The combined organic layers were dried with anhydrous $MgSO_4$ and concentrated to give a crude product. Further purification by silica gel column chromatography with *c*-hexane/EtOAc (15:1→10:1) yielded **2** (2.74 g, 75%). ^{1}H NMR (500 MHz, [D$_6$]DMSO, 25 °C, TMS): δ = 1.27 (t, ^3J = 7.1 Hz, 3H, CH$_3$), 4.29 (q, ^3J = 7.0 Hz, 2H, CH$_2$), 5.98 (s, 2H, CH$_2$), 6.54 (t, ^3J = 7.5 Hz, 1H, CH), 7.04 (t, ^3J = 7.3 Hz, 1H, CH), 7.23 (t, ^3J = 9.7 Hz, 1H, CH), 7.30 (m, 1H), 7.66 (s, 1H, CH), 7.82 (d, ^3J = 9.2 Hz, 1H, CH), 8.17 (dd, ^3J = 9.2, 1.7 Hz, 1H, CH), 8.79 ppm (s, 1H, CH); ^{13}C NMR (500 MHz, [D$_6$]DMSO, 25 °C, TMS): δ = 14.0, 27.6, 42.4, 61.1, 112.0, 113.1, 115.3, 115.5, 119.9, 124.7, 127.3, 129.4, 130.7, 141.6, 142.0, 158.5, 160.4, 160.5 ppm; LC–MS *m/z*: 343 [M^+], t_R = 3.02 min; HR MS *m/z*: calcd. for $C_{18}H_{17}FN_2O_2$ [M^+]: 343.1089, found 343.1084.

3: Pd/C (10%, 0.622 g, 0.584 mmol) and ammonium formate (2.21 g, 35.1 mmol) were added to a solution of **2** (2.00 g, 5.84 mmol) in EtOAc/THF, and the mixture was stirred at reflux for 4 h. The mixture was filtered through a celite pad and the filtrate was concentrated in vacuo to give pure amine **3** (1.73 g, 95%). ^{1}H NMR (500 MHz, [D$_6$]DMSO, 25 °C, TMS): δ = 1.24 (t, ^3J = 7.1 Hz, 3H, CH$_3$), 4.21 (q, ^3J = 7.0 Hz, 2H, CH$_2$), 4.81 (s, 2H, CH$_2$), 5.79 (s, 2H, CH$_2$), 6.41 (t, ^3J = 7.4 Hz, 1H, CH), 6.74 (d, ^3J = 8.9 Hz, 1H, CH), 6.78 (s, 1H, CH), 6.99 (t, ^3J = 7.1 Hz, 1H, CH), 7.10 (s, 1H, CH), 7.22 ppm (m, 3H); ^{13}C NMR (500 MHz, [D$_6$]DMSO, 25 °C, TMS): δ = 14.0, 41.2, 60.0, 103.2, 109.1, 111.1, 115.0, 117.0, 124.4, 125.7, 126.4, 127.2, 128.7, 133.3, 143.0, 158.3, 160.2, 161.1 ppm; LC–MS *m/z*: 313 [M^+], t_R = 1.77 min; HR MS *m/z*: calcd. for $C_{18}H_{17}FN_2O_2$ [M^+]: 313.1347, found 313.1345.

4: Dimethylbutyric acid chloride (3.45 g, 25.6 mmol) in THF at 0 °C was added to a solution of **3** (8.00 g, 25.6 mmol) and triethylamine (2.85 g, 28.2 mmol) in CH_2Cl_2. The mixture was stirred at room temperature overnight. After dilution with CH_2Cl_2, the organic layer was washed with HCl (1 N, aq.) and $NaHCO_3$ (sat., aq.) and concentrated to give the desired amide **4** (5.53 g, 53%). ^{1}H NMR (500 MHz, [D$_6$]DMSO, 25 °C, TMS): δ = 1.04 (s, 9H, 3×CH$_3$), 1.26 (t, ^3J = 7.1 Hz, 3H, CH$_3$), 2.19 (s, 2H, CH$_2$), 4.25 (q, ^3J = 7.1 Hz, 2H, CH$_2$), 5.88 (s, 2H, CH$_2$), 6.42 (t, ^3J = 7.5 Hz, 1H, CH), 7.00 (t, ^3J = 7.5 Hz, 1H, CH), 7.25 (m, 2H), 7.35 (s, 1H, CH), 7.39 (dd, ^3J = 9.0, 1.4 Hz, 1H), 7.49 (d, ^3J = 9.0 Hz, 1H, CH), 8.11 (d, ^3J = 0.7 Hz, 1H, CH), 9.76 ppm (s, 1H, NH); ^{13}C NMR (500 MHz, [D$_6$]DMSO, 25 °C, TMS): δ = 14.0, 29.6, 30.8, 41.5, 49.5, 60.3, 110.6, 110.9, 111.9, 115.0, 119.5, 124.5, 125.3, 127.1, 127.5, 128.9, 133.0, 135.9, 158.3, 160.3, 160.9, 169.6 ppm; LC–MS *m/z*: 411 [M^+], t_R = 2.74 min; HR MS *m/z*: calcd. for $C_{24}H_{27}FN_2O_3$ [M^+]: 411.2709, found 411.2709.

5: LiOH (0.650 g, 26.9 mmol was added to a solution of ethyl ester **4** (5.53 g, 13.5 mmol) in methanol (130.0 mL) and THF (130.0 mL). The mixture was stirred at reflux for 1 h. After cooling to room temperature, HCl (1 N, aq.) was added to the mixture and extracted twice with CH_2Cl_2. The organic layer was dried with anhydrous $MgSO_4$ and concentrated to give acid **5** (4.93 g, 96%). ^{1}H NMR (500 MHz, [D$_6$]DMSO, 25 °C, TMS): δ = 1.03 (s, 9H, 3×CH$_3$), 2.19 (s, 2H, CH$_2$), 5.90 (s, 2H, CH$_2$), 6.41 (t, ^3J = 7.5 Hz, 1H, CH), 7.00 (t, ^3J = 7.3 Hz, 1H, CH), 7.23 (m, 2H), 7.30 (s, 1H, CH), 7.34 (dd, ^3J = 8.9, 1.4 Hz, 1H), 7.43 (d, ^3J = 9.0 Hz, 1H, CH), 8.10 (d, ^3J = 0.8 Hz, 1H, CH), 9.75 ppm (s, 1H, NH); ^{13}C NMR (500 MHz, [D$_6$]DMSO, 25 °C, TMS): δ = 29.6, 30.8, 41.2, 49.5, 110.5, 110.8, 111.9, 115.1, 119.2, 124.5, 125.3, 125.5, 127.1, 128.4, 128.8, 132.8, 135.7, 158.3, 160.3, 162.6, 169.6 ppm; LC–MS *m/z*: 383 [M^+], t_R = 2.22 min; HR MS *m/z*: calcd. for $C_{22}H_{23}FN_2O_3$ [M^+]: 383.1766, found 383.1770.

6: Aniline (102 mg, 1.10 mmol) was added to a mixture of **5** (350 mg, 0.920 mmol), 4-dimethylaminopyridine (55.9 mg, 0.460 mmol), and EDCI (263 mg, 1.37 mmol) in DMF, and the mixture was stirred at room temperature overnight. After dilution with CH_2Cl_2, the resulting solution was washed with HCl (1 N, aq.), water, and brine. The organic layer was dried with anhydrous $MgSO_4$ and concentrated to give a crude material. Further purification by preparative HPLC yielded desired bis-amide **6** (252 mg, 60%) in pure form. ^{1}H NMR (500 MHz, [D$_6$]DMSO, 25 °C, TMS): δ = 1.04 (s, 9H, 3×CH$_3$), 2.20 (s, 2H, CH$_2$), 5.90 (s, 2H, CH$_2$), 6.60 (t, ^3J = 7.5 Hz, 1H, CH), 7.00 (t, ^3J = 7.5 Hz, 1H, CH), 7.09 (t, ^3J = 7.3 Hz, 1H, CH), 7.21 (t, ^3J = 9.9 Hz, 1H, CH), 7.34 (m, 3H), 7.45 (d, ^3J = 8.9 Hz, 1H, CH), 7.72 (d, ^3J = 7.9 Hz, 2H, CH$_2$), 8.10 (s, 1H, CH), 9.75 (s, 1H, NH), 10.36 ppm (s, 1H, NH); ^{13}C NMR (500 MHz, [D$_6$]DMSO, 25 °C, TMS): δ = 29.6, 30.7, 41.2, 49.5, 106.6, 110.7, 111.5, 115.0, 115.2, 118.4, 120.2, 123.6, 124.3, 125.4, 125.6, 127.8, 128.5, 128.9, 131.9, 132.8, 135.1, 138.7, 158.4, 160.2, 160.4, 169.6 ppm; LC–MS *m/z*: 458 [M^+], t_R = 2.30 min; HR MS *m/z*: calcd. for $C_{28}H_{28}FN_3O_2$ [M^+]: 458.2239, found 458.2241.

7: Prepared according to the procedure described for the synthesis of **6** (80%). ^{1}H NMR (500 MHz, [D$_6$]DMSO, 25 °C, TMS): δ = 1.04 (s, 9H, 3×CH$_3$), 2.20 (s, 2H, CH$_2$), 5.86 (s, 2H, CH$_2$), 6.00 (d, ^3J = 2.9 Hz, 1H, CH), 6.50 (t, ^3J = 7.6 Hz, 1H, CH), 6.98 (t, ^3J = 7.4 Hz, 1H, CH), 7.19 (t, ^3J = 9.8 Hz, 1H, CH), 7.25 (m, 1H), 7.42 (d, ^3J = 1.4 Hz, 1H, CH), 7.52 (d, ^3J = 9.0 Hz, 1H, CH), 7.87 (s, 1H, CH), 7.95 (s, 1H, CH), 8.11 (s, 1H, CH), 8.15 (d, ^3J = 2.8 Hz, 1H, CH), 9.78 ppm (s, 1H, NH); ^{13}C NMR (500 MHz, [D$_6$]DMSO, 25 °C, TMS): δ = 29.7, 30.9, 41.8, 49.6, 101.8, 110.9, 112.1, 114.8, 115.2, 119.9, 124.0, 124.5, 125.4, 127.6, 128.3, 129.0, 131.5, 133.1, 135.9, 157.1, 158.5, 159.4, 160.4, 169.7 ppm; LC–MS *m/z*: 448 [M^+], t_R = 2.27 min; HR MS *m/z*: calcd. for $C_{25}H_{26}FN_5O_2$ [M^+]: 448.2144, found 448.2149; m.p. 103 °C.

8: Prepared according to the procedure described for the synthesis of **6** (75%). ^{1}H NMR (500 MHz, [D$_6$]DMSO, 25 °C, TMS): δ = 1.04 (s, 9H, 3×CH$_3$), 2.20 (s, 2H, CH$_2$), 6.05 (s, 2H, CH$_2$), 6.45 (t, ^3J = 7.3 Hz, 1H, CH), 6.99 (t, ^3J = 7.1 Hz, 1H, CH), 7.12 (dd, ^3J = 5.5, 2.9 Hz, 2H, CH$_2$), 7.24 (m, 2H), 7.30 (d, ^3J = 8.6 Hz, 1H, CH), 7.41 (s br, 3H, CH$_3$), 7.57 (s, 1H, CH), 8.14 (s, 1H, CH), 9.74 (s, 1H, NH), 12.23 ppm (s, 1H, NH); ^{13}C NMR (500 MHz, [D$_6$]DMSO, 25 °C, TMS): δ = 29.6, 30.8, 41.5, 49.5, 108.4, 110.6, 111.8, 114.9, 115.1, 118.6, 121.5, 124.4, 125.5, 125.8, 125.9, 127.2, 128.7, 132.7, 135.5, 158.3, 160.2, 169.6 ppm;

LC–MS *m/z*: 498 [M^+], t_R = 2.30 min; HR MS *m/z*: calcd. for $C_{29}H_{28}FN_5O_2$ [M^+]: 498.2300, found 498.2317.

9: Prepared according to the procedure described for the synthesis of **6** (69%). ^{1}H NMR (500 MHz, [D$_6$]DMSO, 25 °C, TMS): δ = 1.04 (s, 9H, 3×CH$_3$), 2.20 (s, 2H, CH$_2$), 5.90 (s, 2H, CH$_2$), 6.60 (t, ^3J = 7.5 Hz, 1H, CH), 7.01 (t, ^3J = 7.5 Hz, 1H, CH), 7.19 (t, ^3J = 9.9 Hz, 1H, CH), 7.25 (m, 1H, CH), 7.37 (dd, ^3J = 8.9, 1.4 Hz, 1H, CH), 7.44 (s, 1H, CH), 7.49 (t, ^3J = 8.9 Hz, 1H, CH), 8.12 (s, 1H, CH), 8.22 (dd, ^3J = 8.7, 2.6 Hz, 1H, CH), 8.74 (d, ^3J = 2.4 Hz, 1H, CH), 9.76 (s, 1H, NH), 10.69 ppm (s, 1H, NH); ^{13}C NMR (500 MHz, [D$_6$]DMSO, 25 °C, TMS): δ = 29.6, 30.7, 41.3, 49.5, 107.4, 110.8, 111.6, 115.0, 118.8, 124.0, 124.4, 125.3, 127.7, 129.0, 130.6, 131.0, 133.0, 135.1, 135.3, 141.2, 143.8, 158.4, 160.4, 169.6 ppm; LC–MS *m/z*: 493 [M^+], t_R = 2.62 min; HR MS *m/z*: calcd. for $C_{27}H_{26}ClFN_4O_2$ [M^+]: 493.1802, found 493.1793.

10: Prepared according to the procedure described for the synthesis of **6** (29%). ^{1}H NMR (500 MHz, [D$_6$]DMSO, 25 °C, TMS): δ = 1.04 (s, 9H, 3 x CH$_3$), 2.19 (s, 2H, CH$_2$), 5.88 (s, 2H, CH$_2$), 6.59 (t, ^3J = 7.5 Hz, 1H, CH), 6.87 (s br, 1H, CH), 6.99 (t, ^3J = 7.4 Hz, 1H, CH), 7.13 (d, ^3J = 8.4 Hz, 1H, CH), 7.18 (t, ^3J = 9.8 Hz, 1H, CH), 7.24 (m, 1H), 7.35 (d, ^3J = 9.0 Hz, 1H, CH), 7.41 (s, 1H, CH), 7.46 (d, ^3J = 9.0 Hz, 1H, CH), 7.70 (t, ^3J = 7.3 Hz, 1H, CH), 7.86 (q, ^3J = 8.8 Hz, 4H), 7.95 (s, 1H, CH), 8.02 (s br, 1H, CH), 8.10 (s, 1H, CH), 9.75 (s, 1H, NH), 10.64 ppm (s, 1H, NH); ^{13}C NMR (500 MHz, [D$_6$]DMSO, 25 °C, TMS): δ = 29.7, 30.8, 41.4, 49.6, 107.5, 110.9, 111.7, 115.1, 115.3, 118.8, 119.6, 124.5, 125.4, 125.6, 127.6, 127.7, 127.8, 128.9, 129.1, 131.4, 133.0, 135.4, 158.5, 160.5, 169.7 ppm; LC–MS *m/z*: 614 [M^+], t_R = 2.33 min; HR MS *m/z*: calcd for $C_{33}H_{32}FN_5O_4S$ [M^+]: 614.2232, found 614.2219.

11: Prepared according to the procedure described for the synthesis of **6** (48%). ^{1}H NMR (500 MHz, [D$_6$]DMSO, 25 °C, TMS): δ = 1.04 (s, 9H, 3×CH$_3$), 2.20 (s, 2H, CH$_2$), 5.92 (s, 2H, CH$_2$), 6.59 (t, ^3J = 7.4 Hz, 1H, CH), 7.01 (t, ^3J = 7.4 Hz, 1H, CH), 7.23 (m, 4H), 7.35 (d, ^3J = 8.4 Hz, 1H, CH), 7.46 (m, 2H), 7.52 (t, ^3J = 8.1 Hz, 1H, CH), 7.69 (d, ^3J = 7.6 Hz, 1H, CH), 7.80 (d, ^3J = 8.6 Hz, 1H, CH), 7.95 (d, ^3J = 8.8 Hz, 2H, CH$_2$), 7.98 (s, 1H, CH), 8.12 (s, 1H, CH), 8.30 (s, 1H, CH), 9.76 (s, 1H, NH), 10.58 (s, 1H, NH), 10.60 ppm (s, 1H, NH); ^{13}C NMR (500 MHz, [D$_6$]DMSO, 25 °C, TMS): δ = 29.6, 30.7, 41.2, 49.5, 107.0, 110.7, 111.6, 115.1, 115.2, 118.6, 119.7, 122.6, 123.4, 124.4, 125.4, 126.4, 127.7, 128.6, 128.8, 128.9, 131.6, 132.9, 135.1, 135.2, 138.6, 138.9, 142.0, 158.4, 160.3, 165.8, 169.6 ppm; LC–MS *m/z*: 656 [M^+], t_R = 2.37 min; HR MS *m/z*: calcd. for $C_{35}H_{34}FN_5O_5S$ [M^+]: 656.2338, found 656.2334.

12: 4-Dimethylaminopyridine (240 mg, 1.96 mmol) and HATU (994 mg, 2.62 mmol) were added to a solution of **5** (500 mg, 1.31 mmol) in DMF. After stirring for 10 min, 5-amino-nicotinic acid methyl ester (298 mg, 1.96 mmol) was added, and the mixture was stirred at room temperature overnight. It was diluted with CH_2Cl_2 and consecutively washed with HCl (1 N, aq.), water, and brine. The organic layer was dried with anhydrous $MgSO_4$ and concentrated to give a crude product. Further purification by preparative HPLC gave amide **12** (411 mg, 61%). ^{1}H NMR (500 MHz, [D$_6$]DMSO, 25 °C, TMS): δ = 1.04 (s, 9H, 3×CH$_3$), 2.20 (s, 2H, CH$_2$), 3.91 (s, 3H, CH$_3$), 5.91 (s, 2H, CH$_2$), 6.61 (t, ^3J = 7.4 Hz, 1H, CH), 7.01 (t, ^3J = 7.3 Hz, 1H, CH), 7.20 (t, ^3J = 9.6 Hz, 1H, CH), 7.26 (m, 1H), 7.37 (d, ^3J = 8.8 Hz, 1H, CH), 7.48 (s br, 2H, CH$_2$), 8.13 (s, 1H, CH), 8.76 (s, 1H, CH), 8.81 (s, 1H, CH), 9.12 (s, 1H, CH), 9.77 (s, 1H, NH), 10.77 ppm (s, 1H, NH); ^{13}C NMR (500 MHz, [D$_6$]DMSO, 25 °C, TMS): δ = 29.7, 30.8, 41.5, 49.6, 52.5, 107.6, 110.9, 111.7, 115.3, 118.9, 124.5, 125.4, 126.9, 127.8, 129.1, 131.0, 133.1, 135.4, 135.7, 144.6, 145.2, 158.5, 160.5, 160.8, 165.1, 169.7 ppm; LC–MS *m/z*: 517 [M^+], t_R = 2.35 min; HR MS *m/z*: calcd. for $C_{29}H_{29}FN_4O_4$ [M^+]: 517.2246, found 517.2239.

13: LiOH (13.9 mg, 0.58 mmol) in water (0.5 mL) was added to a solution of **12** (150 mg, 0.290 mmol) in THF (2.5 mL) and MeOH (2.5 mL). The mixture was stirred at 90 °C for 2 h. The resulting solution was acidified to pH 6 with HCl (1 N, aq.), and extracted with CH_2Cl_2 three times. The organic layer was dried with anhydrous Na_2SO_4 and concentrated to give carboxylic acid **13** (131 mg, 90%). ^{1}H NMR (500 MHz, [D$_6$]DMSO, 25 °C, TMS): δ = 1.03 (s, 9H, 3×CH$_3$), 2.18 (s, 2H, CH$_2$), 5.90 (s, 2H, CH$_2$), 6.60 (t, ^3J = 7.5 Hz, 1H, CH), 7.00 (t, ^3J = 7.3 Hz, 1H, CH), 7.23 (m, 2H), 7.36 (d, ^3J = 8.6 Hz, 1H, CH$_2$), 7.46 (m, 2H), 8.11 (s, 1H, CH), 8.71 (s, 1H, CH), 8.78 (s, 1H, CH), 9.08 (d, ^3J = 1.7 Hz, 1H, CH), 9.76 (s, 1H, CH), 10.73 (s, 1H, CH), 13.47 ppm (s br, 1H, CH); ^{13}C NMR (500 MHz, [D$_6$]DMSO, 25 °C, TMS): δ = 29.6, 30.7, 42.0, 49.5, 107.5, 110.8, 111.6, 115.2, 118.8, 124.4, 125.3, 126.4, 127.2, 127.8, 129.0, 131.0, 133.0, 135.3, 144.8, 158.4, 160.4, 160.6, 166.1, 169.6 ppm; LC–MS *m/z*: 503 [M^+], t_R = 2.12 min; HR MS *m/z*: calcd. for $C_{28}H_{27}FN_4O_4$ [M^+]: 503.2090, found 503.2075.

14: 4-Dimethylaminopyridine (18.2 mg, 0.150 mmol) and HATU (75.7 mg, 0.200 mmol) were added to a solution of **13** (50.0 mg, 0.100 mmol) in DMF. After stirring for 10 min, a solution of sulfanylamide (22.3 mg, 0.130 mmol) in DMF was added dropwise, and stirred at room temperature overnight. The mixture was diluted with water and extracted with CH_2Cl_2 three times. The combined organic layers were dried with anhydrous $MgSO_4$ and concentrated to give a crude product. Further purification by preparative HPLC yielded pure carboxamide **14** (34.8 mg, 53%). ^{1}H NMR (500 MHz, [D$_6$]DMSO, 25 °C, TMS): δ = 1.04 (s, 9H, 3×CH$_3$), 2.20 (s, 2H, CH$_2$), 5.92 (s, 2H, CH$_2$), 6.61 (t, ^3J = 7.4 Hz, 1H, CH), 7.02 (t, ^3J = 7.3 Hz, 1H, CH), 7.20 (t, ^3J = 9.6 Hz, 1H, CH), 7.26 (m, 1H), 7.31 (s, 1H, CH), 7.37 (d, ^3J = 8.8 Hz, 1H, CH), 7.48 (d, ^3J = 7.2 Hz, 2H, CH$_2$), 7.82 (d, ^3J = 8.6 Hz, 2H, CH$_2$), 7.94 (d, ^3J = 8.6 Hz, 2H, CH$_2$), 8.14 (s, 1H, CH), 8.67 (s, 1H, CH), 8.87 (s, 1H, CH), 9.09 (s, 1H, CH), 9.77 (s, 1H, CH), 10.78 ppm (d, ^3J = 9.1 Hz, 2H, CH$_2$); ^{13}C NMR (500 MHz, [D$_6$]DMSO, 25 °C, TMS): δ = 29.6, 30.7, 41.3, 49.5, 107.5, 110.8, 111.6, 115.2, 118.8, 119.9, 124.4, 125.3, 126.2, 126.5, 127.7, 129.0, 130.2, 131.0, 133.0, 135.4, 139.0, 141.6, 143.2, 144.2, 158.4, 160.4, 160.6, 164.2, 169.6 ppm; LC–MS *m/z*: 657 [M^+], t_R = 2.30 min; HR MS *m/z*: calcd. for $C_{34}H_{33}FN_6O_5S$ [M^+]: 657.2290, found 657.2282.

Computational chemistry: A homology model of ECE was created by using an X-ray crystallographic structure of the NEP–phosphoramidon complex (PDB: 1DMT) as the template in a manner similar to an approach reported by Bur et al.[27] Each of the amino acids in the NEP structure was replaced with the corresponding residue in the ECE sequence by using SYBYL 6.9 (Triopos Inc.). The sequences of the two enzymes were aligned using a previously reported method.[27] The replacement of amino acids was done to preserve the coordinates of the original NEP structure as much as possible. The structures of the loop regions were constructed by the loop search algorithm implemented in SYBYL. The resultant model structure was then energy-minimized with MMFF94s force field implemented in SYBYL with a distance-dependent dielectric constant 4r.

Docking of indole **11** to the ECE model: First, the structure of **11** was flexibly aligned on the structure of the phosphoramidon bound to the NEP X-ray crystal structure, by using a program developed in-house (FAME). The aligned structure was then transferred to the active site of the ECE model by superposing the NEP structure onto the ECE model. The structure of the compound and the amino acids in the active site were energy-minimized with

MMFF94s force field implemented in SYBYL with a distance-dependent dielectric constant 4r.

Big-hET-1 pressure response in anaesthetized rats: All studies performed in anaesthetized rats were approved by the Regierungspräsident Düsseldorf (VVH 400A40). Male Wistar rats with a body weight of 300–350 g were anaesthetized with intraperitoneal injections of thiopental (100 mg kg^{-1}). Following tracheotomy, a catheter for monitoring blood pressure and heart frequency was introduced into the femoral artery, and a catheter for substance administration was introduced into the femoral vein. The animals were ventilated with normal air and body temperature was monitored. Ganglia blockade was initiated by intravenous administration of pentolinium (5 mg kg^{-1}) in a volume of 1 mL kg^{-1}. After 2 min, the test substances were administered intravenously in a solution of Transcutol/Cremophor/physiological NaCl solution 0.9% (10:10:80 *w/w/w*) in a volume of 1 mL kg^{-1}. Big-hET-1 was administered as an intravenous bolus injection at a dose of 9 μg kg^{-1} in a volume of 1 mL kg^{-1} 1 min after substance administration. The hemodynamic parameters were monitored for 30 min.

Dahl S rat model: Inbred Dahl rats, which were bred selectively for sensitivity (S rats), or resistance (R rats) to the hypertensive action of a high-salt diet were used to study the effect of ECE inhibitors. At the age of eight weeks, the animals were fed a diet high in NaCl (8% in commercial feed, Sniff, Soest, Germany) for four weeks as described previously.[29] The animals were anaesthetized with thiopental "Nycomed" (100 mg kg^{-1} intraperitoneal, Nycomed, Munich, Germany). A tracheotomy was performed, and catheters were inserted into the femoral artery for blood pressure and heart rate measurements (Gould pressure transducer and recorder, model RS 3400), and into the femoral vein for substance administration. The animals were ventilated with room air and body temperature was controlled. For intravenous administration, the substances were dissolved as described above. The hemodynamic parameters were monitored for 60 min.

Mouse model of myocardial infarction: Oral application of the test substance or control solution was performed on conscious animals ≈30 min prior to anesthesia. Anesthesia was induced by intraperitoneal injection of the following solution: part 1: Fentanyl (0.475 mL, final concentration 0.05 mg mL^{-1}), Midazolam (Ratiopharm, Ulm, Germany) (1.600 mL, final concentration 0.27 mg mL^{-1}), and Dormitor (Pfizer, Karlsruhe, Germany) (0.400 mL, final concentration 0.0013 mg mL^{-1}) diluted with physiological NaCl solution (30 mL); part 2: Avertin (tribromoethanol, 25 g, Aldrich, Munich, Germany), *tert*-amyl alcohol (10 mL, Merck, Darmstadt, Germany); this solution was mixed 1:40 with drinking water or physiological NaCl solution prior to use. Part 1 (15 μL g^{-1} body weight) and part 2 (300 μL per mouse) was mixed in a one-way syringe (1 mL volume) prior to intraperitoneal application. Deep anesthesia normally takes 2–5 min.

Anaesthetized CD1 mice were shaved on the left thorax prior to surgery. The mice were then intubated, and artificial respiration was performed with a Mini Vent Typ 845 (Hugo Sachs Elektronik, March-Hugstetten, Germany). Ventilation was kept at a frequency of 110 strokes min^{-} with a volume of 300 μL. Body temperature was controlled by a rectal temperature sensor GMH3230 (Greisinger Electronic, Regenstauf, Germany). Control of the body temperature was maintained by an electric heating pad within the range of 36.5–37.5 °C. Electrodes were placed to register the electrocardiogram (ECG) by an ECG device connected to a Dash 4μ recorder (Astromed, West Warwick, RI, USA). Survival was monitored by the ECG register. A short control record was stored prior to the surgical procedure.

Surgery started with a cut (≈10 mm) of the skin starting at the left foreleg in the direction of the hind leg. The underlying soft tissue and muscles were then cut. The thorax was opened wide between the second and third rib. After opening the pericard, a channel was pierced under left coronary artery (LAD) with a surgical needle holder carrying an Ethicon-Prolene-TF-6 6/0 thread EH 7914E (Ethicon, Brussels, Belgium). The thread was placed about 2 mm distal of the atrium base.

The induction of a myocardial infarct started 45 min after substance application by occlusion of the LAD. The LAD was occluded by a double knot in the surgical thread. The thorax was closed by a continuous suture. The experiments ended with the death of the animal or were finished 2 h after occlusion of the LAD.

Acknowledgments

We thank B. Burghard, M. Eckardt, E. Eisfelder, C. Fischer, R. Hartkopf, B. R. Hartmann, R. Jawulski, N. Krüger, and I. Limberg for technical assistance, and Dipl.-Ing. H. Musche and Dr. P. Schmitt for the recording of analytical data. Special thanks go to Dr. A. Hillisch for a critical review of the manuscript. We are grateful to Dr. J. Hütter, Dr. J. Mittendorf and Dr. H. Wild for helpful discussions and their continued support.

Keywords: enzymes · heart diseases · indoles · inhibitors · synthetic drugs

[1] M. Yanagisawa, H. Kurihara, S. Kimura, Y. Tomobe, M. Kobayashi, Y. Mitsui, Y. Yazaki, K. Goto, T. Masaki, *Nature* **1988**, *332*, 411–415.
[2] For a review, see: T. Masaki, *Trends Pharmacol. Sci.* **2004**, *25*, 219–224.
[3] a) E. L. Schiffrin, L. Y. Deng, P. Sventek, R. Day, *J. Hypertens.* **1997**, *15*, 57–63. b) C. E. Lemne, T. Lundeberg, E. Theodorsson, U. De Faire, *J. Hypertens.* **1994**, *12*, 1069–1074.
[4] S. Ergul, D. C. Parish, D. Puett, A. Ergul, *Hypertension* **1996**, *28*, 652–655.
[5] D. Aronson, A. J. Burger, *Pacing Clin. Electrophysiol.* **2003**, *26*, 703–710.
[6] D. J. Stewart, G. Kubac, K. B. Costello, P. Cernacek, *J. Am. Coll. Cardiol.* **1991**, *18*, 38–43.
[7] C. Ihling, T. Szombathy, B. Bohrmann, M. Brockhaus, H. E. Schaefer, B. M. Löffler, *Circulation* **2001**, *104*, 864–869.
[8] A. Giaid, M. Yanagisawa, D. Langleben, R. P. Michel, R. Levy, H. Shennib, S. Kimura, T. Masaki, W. P. Duguid, D. J. Stewart, *N. Engl. J. Med.* **1993**, *328*, 1732–1739.
[9] H. Krum, D. Liew, *Curr. Opin. Invest. Drugs* **2003**, *4*, 298–302.
[10] M. Kirchengast, M. Luz, *J. Cardiovasc. Pharmacol.* **2005**, *45*, 182–291.
[11] B. J. Nelson, *J. Urol.* **2003**, *170*, S65–S68.
[12] A. Jimeno, M. Carducci, *Expert Opin. Invest. Drugs* **2004**, *13*, 1631–1640.
[13] A. Schweizer, O. Valdenaire, P. Nelböck, U. Deuschle, J.-B. Dumas Milne Edwards, J. G. Stumpf, B. M. Löffler, *Biochem. J.* **1997**, *328*, 871–877.
[14] A. Schröder, M. Tajimi, H. Matsumoto, C. Schröder, M. Brands, K. E. Andersson, *J. Urol.* **2004**, *172*, 1171–1174.
[15] N. E. Mealy, M. Bayes, M. Del Fresno, *Drugs Future* **2001**, *26*, 1149–1154.
[16] H. Cohen, C. Chahine, A. Hui, R. Mukherji, *Am. J. Health-Syst. Pharm.* **2004**, *61*, 1107–1119.
[17] K. Chin, R. Channick, *Expert Rev. Cardiovasc. Ther.* **2004**, *2*, 175–182.
[18] D. Xu, N. Emoto, A. Giaid, C. Slaughter, S. Kaw, D. deWit, M. Yanagisawa, *Cell* **1994**, *78*, 473–485.
[19] S. A. Dogrell, *Expert Opin. Ther. Pat.* **2004**, *14*, 655–665.
[20] A. Y. Jeng, *Curr. Opin. Invest. Drugs* **2003**, *4*, 1076–1081.
[21] S. De Lombaert, L. Blanchard, L. B. Stamford, J. Tan, E. M. Wallace, Y. Satoh, J. Fitt, D. Hoyer, D. Simonsbergen, J. Moliterni, N. Marcopoulos, P.

Savage, M. Chou, A. J. Trapani, A. Y. Jeng, *J. Med. Chem.* **2000**, *43*, 488 – 504.
[22] D. N. Muller, A. Mullaly, R. Dechend, J.-K. Park, A. Fiebeler, B. Pilz, B. M. Loeffler, D. Blum-Kaelin, S. Masur, H. Dehmlow, J. D. Aebi, H. Haller, F. C. Luft, *Hypertension* **2002**, *40*, 840 – 846.
[23] K. Umekawa, H. Hasegawa, Y. Tsutsumi, K. Sato, Y. Matsumura, N. Ohashi, *Jpn. J. Pharmacol.* **2000**, *84*, 7 – 15.
[24] A. Y. Jeng, S. De Lombaert, M. E. Beil, C. W. Bruseo, P. Savage, M. Chou , A. J. Trapani, *J. Cardiovasc. Pharmacol.* **2000**, *36* (5 suppl. 1), S36 – S39.
[25] J. K. Ergueden, T. Krahn, C. Schröder, J.-P. Stasch, S. Weigand, H. Wild, M. Brands, S. Siegel, D. Heimbach, J. Keldenich (Bayer AG), WO 03/28719, **2003** [*Chem. Abstr.* **2003**, *138*, 304157].
[26] M. Brands, J. K. Ergüden, K. Hashimoto, D. Heimbach, C. Schröder, S. Siegel, J.-P. Stasch, S. Weigand, *Bioorg. Med. Chem. Lett.* **2005**, *15*, 4201 – 4205.
[27] D. Bur, G. E. Dale, C. Oefner, *Protein Eng.* **2001**, *14*, 337 – 341.
[28] D. F. Veber, S. R. Johnson, H. Y. Cheng, B. R. Smith, K. W. Ward, K. D. Kopple, *J. Med. Chem.* **2002**, *45*, 2615 – 2623.
[29] J.-P. Stasch, S. Kazda, C. Hirth-Dietrich, D. Neuser, *Clin. Exp. Hypertens. Part A* **1990**, *12*, 1419 – 1436.
[30] T. I'keda, H. Ohta, M. Okada, N. Kawai, R. Nakao, P. K. Siegl, T. Kobayashi, S. Maeda, T. Miyauchi, M. Nishikibe, *Hypertension* **1999**, *34*, 514 – 519.
[31] K. Sogabe, H. Nirei, M. Shoubo, A. Nomoto, S. Ao, Y. Notsu , T. Ono, *J. Pharmacol. Exp. Ther.* **1993**, *264*, 1040 – 1046.

Received: July 15, 2005
Published online on October 27, 2005

